

Hamilton-Jacobi Reachability Analysis for Hybrid Systems with Controlled and Forced Transitions

Javier Borquez¹, Shuang Peng¹, Yiyu Chen¹, Quan Nguyen¹, Somil Bansal¹

Abstract—Hybrid dynamical systems with non-linear dynamics are one of the most general modeling tools for representing robotic systems, especially contact-rich systems. However, providing guarantees regarding the safety or performance of such hybrid systems can still prove to be a challenging problem because it requires simultaneous reasoning about continuous state evolution and discrete mode switching. In this work, we address this problem by extending classical Hamilton-Jacobi (HJ) reachability analysis, a formal verification method for continuous non-linear dynamics in the presence of bounded inputs and disturbances, to hybrid dynamical systems. Our framework can compute reachable sets for hybrid systems consisting of multiple discrete modes, each with its own set of non-linear continuous dynamics, discrete transitions that can be directly commanded or forced by a discrete control input, while still accounting for control bounds and adversarial disturbances in the state evolution. Along with the reachable set, the proposed framework also provides an optimal continuous and discrete controller to ensure system safety. We demonstrate our framework in simulation on an aircraft collision avoidance problem, as well as on a real-world testbed to solve the optimal mode planning problem for a quadruped with multiple gaits.

I. INTRODUCTION

Hybrid dynamical system is a popular and versatile tool to model robotic systems that exhibit both continuous and discrete dynamics [1], [2]. For example, for a legged robot, the swinging of a leg has continuous dynamics, whereas contacts with ground are well-modeled as discrete events. However, as with many advanced modeling tools, their very complexity and richness presents challenges, particularly when it comes to ensuring safety and performance for such systems. Designing safe controllers for hybrid dynamical systems demands simultaneous reasoning about the continuous evolution of states and the discrete mode transitions, a task that can quickly become computationally intensive and conceptually challenging.

Reachability analysis is a powerful and effective approach for analyzing and controlling hybrid dynamical systems. It provides a comprehensive understanding of the system's behavior by characterizing the Backward Reachable Tube (BRT) of the system – the set of all possible initial states that can eventually reach some set of target states under optimal control actions. If the target set represents the undesirable states for the system, the BRT represents the set of states that are potentially unsafe for the system and should be avoided. The converse of the BRT thus provides a safe operation region for the system. Reachability analysis for hybrid dynamical systems has been studied using a variety of different frameworks, such as zonotopes [3]–[6], hybrid denotable sets [7], [8], Taylor models [9]–[11], satisfiability modulo theory [12], [13], support functions [14]–[16], timed

automata [17] and linear hybrid automata [17]–[20], among others. However, these methods typically impose restrictive assumptions on the system, such as limiting the analysis to linear continuous dynamics, not accounting for discrete control switches, bounding the number of mode changes, not allowing continuous controls, or not considering disturbances and dynamics uncertainty. Moreover, most of these methods only provide an over-approximation of the BRT.

Another approach for computing BRT for hybrid dynamical systems is via Hamilton-Jacobi (HJ) Reachability analysis. Its advantages include compatibility with general non-linear system dynamics, formal treatment of bounded disturbances, and the ability to deal with state and input constraints [21]. Several works have addressed the control and safety analysis of hybrid dynamical systems through HJ Reachability [22]–[26]. However, these methods often rely on hand and hard-coded heuristics to account for discrete mode switching. Moreover, the BRT computation relies on an iterative refinement that may not necessarily converge. One particular work for the computation of region-of-attraction and stabilizing controllers for walking robots has at its core a generalization of the HJ reachability framework to account for discontinuous state changes originating from state resets [27]. However, generalizing the HJ reachability framework for multiple discrete modes and accounting for discrete controls still remains challenging.

In this work, we propose a general HJ reachability framework for hybrid dynamical systems. Our framework formulates the BRT computation for hybrid systems as a robust optimal control problem. Using the principle of dynamic programming, we simultaneously reason about optimal continuous and discrete control inputs for this optimal control problem, resulting in a generalized version of Hamilton-Jacobi-Bellman equation. We demonstrate that the existing numerical algorithms to compute BRTs can easily be extended to compute this generalized value function, thereby providing both the BRT as well as the safe discrete and continuous control inputs for the hybrid system. Our framework can handle hybrid systems consisting of multiple discrete modes with nonlinear dynamics, discrete control switches that allow or force transitions between different discrete modes, (discontinuous) state resets upon discrete switches, control bounds, as well as, potentially adversarial, disturbances. We demonstrate the efficacy of our framework in simulation and on a real-world quadruped testbed.

II. PROBLEM FORMULATION

Consider a hybrid dynamical system with a finite set of discrete modes $Q = \{q_1, q_2, \dots, q_N\}$, connected through

¹Authors are with the University of Southern California, LA, USA.

controlled or forced switches. We also refer to q_i as the discrete state of the system. Let $x \in X \subset \mathbb{R}^{n_x}$ be the continuous

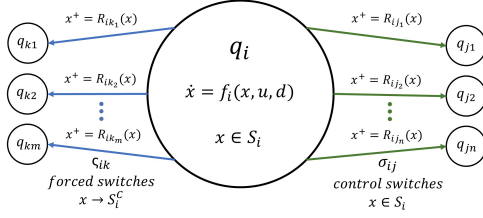


Fig. 1: Hybrid dynamical system with controlled and forced transitions.

state of the system, $u \in U \subset \mathbb{R}^{n_u}$ be the continuous control input, and $d \in D \subset \mathbb{R}^{n_d}$ be the continuous disturbance in the system. In each discrete mode $q_i \in Q$, the continuous state evolves according to the dynamics: $\dot{x} = f_i(x, u, d)$, as long as $x \in S_i \subset X$. Here, S_i is the valid operation domain for mode q_i . q_i also has discrete control switches σ_{ij} that allow *controlled transition* into another discrete mode q_j , where $j \in \{j_1, j_2, \dots, j_n\} \subset \{1, 2, \dots, N\}$. Note that the number of discrete modes the system can transition into (that is, n) may vary across different q_i . As x approaches S_i^C (denoted $x \rightarrow S_i^C$), the system must take one of the forced control switches, ς_{ik} . This leads to a *forced transition* into another discrete modes q_k where $k \in \{k_1, k_2, \dots, k_m\} \subset \{1, 2, \dots, N\}$. Each discrete transition from q_i to q_j , whether controlled or forced, might lead to a state reset $x^+ = R_{ij}(x)$, where x is the state before the transition, x^+ is the state after the transition.

Our key objective in this work is to compute the **Backward Reachable Tube (BRT)** of this hybrid dynamical system, defined as the set of initial discrete modes and continuous states (x, q) of the system for which the agent acting optimally and under worst-case disturbances will eventually reach a target set \mathcal{L} within the time horizon $[t, T]$. Mathematically, the BRT is defined as:

$$\mathcal{V}(t) = \{(x_0, q_0) : \forall d(\cdot), \exists u(\cdot), \sigma(\cdot), \varsigma(\cdot), \exists s \in [t, T], x(s) \in \mathcal{L}\},$$

where $x(s)$ denotes the (continuous) state of the system at time s , starting from state x_0 and discrete mode q_0 under continuous control profile $u(\cdot)$, discrete control switch profile $\sigma(\cdot)$ ¹, forced control switch profile $\varsigma(\cdot)$, and disturbance $d(\cdot)$. Along with the BRT, we are interested in finding the optimal discrete and continuous control inputs that steer the system to the target set.

Conversely, if \mathcal{L} represents the set of undesirable states for the system (such as obstacles for a navigation robot), we are interested in computing the BRT with the role of control and disturbance switched, i.e., finding the set of initial states from which getting into \mathcal{L} is unavoidable, despite best control effort.

Running example (Dog1D): To illustrate our approach, we will use the following running example throughout this paper. We consider very simplified, high-level dy-

¹If there is no discrete control being leveraged at time s , $\sigma(s)$ or $\varsigma(s)$ can be thought of a “dummy” discrete control that keeps the system in the current discrete mode.

namics for a robot quadruped moving in one dimension in a room with an obstacle (table).

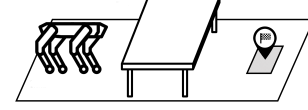


Fig. 2: A simple 1D longitudinal navigation scenario.

The robot goal is to reach the marked area on the other side of the table as shown in Fig. 2. The hybrid system representation of this system is shown in Fig. 3:

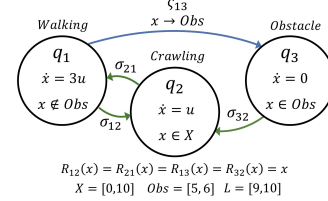


Fig. 3: Dog1D hybrid system formulation.

Here, the continuous state $x \in \mathbb{R}$ is the position of the robot and q_i with $i \in \{1, 2, 3\}$ are the discrete modes of the system. $u \in [0, 1]$ is the continuous control of the system. The target set is given as the set of positions $9 \leq x \leq 10$.

In this example, q_1 represents a walking gait, q_3 represents frozen dynamics when the walking robot comes in contact with the table obstacle, and q_2 is a crawling gait that allows the robot to move under the table but at a slower rate compared to walking. The BRT for this example corresponds to all the combinations of continuous states and discrete modes (x, q) from which the quadruped can reach the target set within a 5 second time horizon.

III. BACKGROUND: HAMILTON-JACOBI REACHABILITY

One way to compute the BRT for continuous dynamical systems is through Hamilton-Jacobi (HJ) reachability analysis. To illustrate HJ reachability, we assume that the system has only one discrete mode, i.e., there are no discrete transitions.

In HJ reachability, the BRT computation is formulated as a zero-sum game between control and disturbance. This results in a robust optimal control problem that can be solved using the dynamic programming principle. First, a target function $l(x)$ is defined whose sub-zero level set is the target set \mathcal{L} , i.e. $\mathcal{L} = \{x : l(x) \leq 0\}$. The BRT seeks to find all states that could enter \mathcal{L} at any point within the time horizon. This is computed by finding the minimum distance to \mathcal{L} over time:

$$J(x, t, u(\cdot), d(\cdot)) = \min_{\tau \in [t, T]} l(x(\tau)) \quad (1)$$

Our goal is to capture this minimum distance for optimal system trajectories. Thus, we compute the optimal control that minimizes this distance (drives the system towards the target) and the worst-case disturbance signal that maximizes the distance. The value function corresponding to this robust optimal control problem is:

$$V(x, t) = \sup_{d(\cdot)} \inf_{u(\cdot)} \{J(x, t, u(\cdot), d(\cdot))\}. \quad (2)$$

The value function in (2) can be computed using dynamic programming, which results in the following final value Hamilton-Jacobi-Isaacs Variational Inequality (HJI-VI):

$$\min \{D_t V(x, t) + \mathcal{H}(x, t), l(x) - V(x, t)\} = 0 \quad (3)$$

$$V(x, T) = l(x)$$

D_t and ∇ represent the time and spatial gradients of the value function. \mathcal{H} is the Hamiltonian, which optimizes over the inner product between the spatial gradients of the value function and the dynamics to compute the optimal control and disturbance:

$$\mathcal{H}(x, t) = \max_{d \in D} \min_{u \in U} \nabla V(x, t) \cdot f(x, u, d). \quad (4)$$

The term $l(x) - V(x, t)$ in (3) restricts system trajectories that enter and leave the target set, enforcing that any trajectory with a negative distance at any time will continue to have a negative distance for the rest of the time horizon. Once the value function is obtained, the BRT is given as the sub-zero level set of the value function:

$$\mathcal{V}(t) = \{x : V(x, t) \leq 0\} \quad (5)$$

The corresponding optimal control can be derived as:

$$u^*(x, t) = \arg \min_{u \in U} \max_{d \in D} \nabla V(x, t) \cdot f(x, u, d) \quad (6)$$

The system can guarantee reaching the target set as long as it starts inside the BRT and applies the optimal control in (6) at the BRT boundary. The optimal adversarial disturbance can be similarly obtained as (6).

This formulation can be used to provide safety guarantees by switching the roles of the control and disturbance in (4). In that case, the BRT represents the states that will be driven into the target by optimal disturbance even if we apply optimal control, so safety can be maintained as long as the system stays outside the BRT and applies optimal control at the boundary.

However, one of the key limitations of HJ reachability analysis is that it assumes continuous dynamics and does not account for discrete mode switching or state resets. Overcoming this limitation is the core focus of this work.

Running example (DogID): Computing the BRT for the running example using the classical Hamilton-Jacobi formulation with no optimal discrete mode switches gives the results shown in Fig. 4.

For the crawling gait it can be observed that the BRT (the blue shaded area) propagates through the obstacle and the BRT includes $x = 4m$ because the system can move at $1m/s$ reaching the boundary of the target in exactly $5s$. For the walking wait, even though the system is allowed to move faster, the BRT stops at the boundary of the obstacle as the walking gait gets stuck, so only states that start from the right side of the obstacle can reach the target set.

If we imagine the system being able to transition optimally between the discrete modes, it would only crawl for states in the obstacle and walk elsewhere, allowing to

reach states farther to the left. As we demonstrate later, the proposed framework can reason about such optimal transitions.

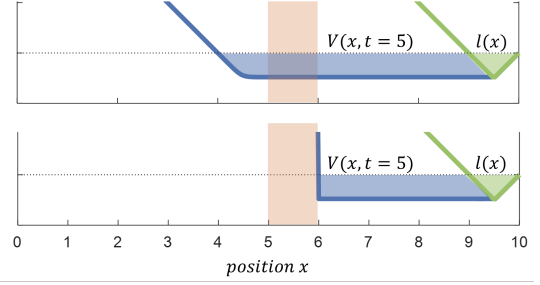


Fig. 4: (Top) Value function for crawling gait mode. (Bottom) Value function for walking gait mode. Obstacle is shown in shaded red. Blue shade shows BRT as the subzero level of the value function. Green shade shows target set as the subzero level of $l(x)$.

IV. HJ REACHABILITY FOR GENERAL HYBRID SYSTEMS

The core contribution of this work is Theorem 1, an extension of the classical HJ reachability framework to hybrid dynamical systems with controlled and forced transitions, as well as state resets.

Theorem 1: For a hybrid dynamical system, the value function $V(x, q_i, t)$ that captures the BRT for an implicit target function $l(x)$ is given by solving the following constrained VI. If $x \in S_i$:

$$\min \{l(x) - V(x, q_i, t), \min_{\sigma_{ij}} V(R_{ij}(x), q_j, t) - V(x, q_i, t),$$

$$D_t V(x, q_i, t) + \max_{d \in D} \min_{u \in U} \nabla V(x, q_i, t) \cdot f_i(x, u, d)\} = 0,$$

and if $x \in S_i^C$, $V(x, q_i, t) = \min_{\varsigma_{ik}} V(R_{ik}(x), q_k, t)$, with terminal time condition:

$$V(x, q_i, T) = l(x) \quad (7)$$

Intuitively, Theorem 1 updates the value function for each discrete mode q_i with the optimal value across the discrete modes it can transition to. For states inside the operation domain S_i , this corresponds to taking one of the control switches σ_{ij} with their corresponding reset maps $R_{ij}(x)$ or staying in the operation mode q_i itself, which will lead to a continuous flow of the value function, similar to (3). In contrast, for states outside the operation mode domain δS_i^C , the system has to take a forced switch ς_{ik} with their corresponding reset maps $R_{ik}(x)$. Thus, the optimal value function is given by the one that takes the system to the minimum value upon the discrete transition. The proof of Theorem 1 formalizes this intuition using the Bellman principle of optimality, the detail of the proof can be found on the Appendix. Once we compute the value function, the BRT for the hybrid system is given as:

$$\mathcal{V}(t) = \{(x, q) : V(x, q, t) \leq 0\} \quad (8)$$

Finally, the optimal discrete and continuous controls at state (x, q_i) at time t are given as:

$$u^*(x, q_i, t) = \arg \min_{u \in U} \max_{d \in D} \nabla V(x, q_i, t) \cdot f_i(x, u, d)$$

$$\sigma_{ij}^*(x, q_i, t) = \arg \min_{\sigma_{ij}} V(R_{ij}(x), q_j, t) \text{ if } x \in S_i \quad (9)$$

$$\varsigma_{ik}^*(x, q_i, t) = \arg \min_{\varsigma_{ik}} V(R_{ik}(x), q_k, t) \text{ if } x \in S_i^C,$$

where, for completeness, we add a “dummy” discrete control σ_{ii} that keeps the system in the same discrete mode.

Remark 1: Note that the proposed framework can easily be extended to scenarios where the forced transitions cannot be controlled and represent adversarial or uncertain transitions instead. In this case, we can use max instead of min over ς_{ik} in Theorem 1 to account for the worst-case behavior.

Numerical implementation: We now present a numerical algorithm that can be used to calculate the value function in Theorem 1. It builds upon the value function calculation for the classical HJI-VI in (2), which is solved using currently available level set methods [28]. Specifically, the value function is computed over a discretized state-space grid and is propagated in time using a small timestep δ . After each propagation step, the value function is updated for all (x, q) using Theorem 1, until the time horizon T is reached.

Algorithm 1: Value function computation for hybrid dynamical system

Input: $l(x), T, \delta$
Output: $V(x, q_i, t) \forall i$
Initialization: $V(x, q_i, T) = l(x) \forall i; \quad t = T$
while $(t > 0)$ **do**
 foreach $(q_i \in Q)$ **do**
 $V(x, q_i, t - \delta) = V(x, q_i, t) +$
 $\max_d \min_u \nabla V(x, q_i, t) \cdot$
 $f_i(x, u, d) \delta$
 foreach $(q_i \in Q)$ **do**
 if $(x \in S_i)$ **then**
 $V(x, q_i, t - \delta) = \min\{l(x), V(x, q_i, t - \delta),$
 $\min_{\sigma_{ij}} V(R_{ij}(x), q_j, t -$
 $\delta)\}$
 else if $(x \in S_i^C)$ **then**
 $V(x, q_i, t - \delta) = \min_{\varsigma_{ik}} V(R_{ik}(x), q_k, t - \delta)$
 $t = t - \delta$

It is important to stress the remarkable similarity of this new hybrid reachability algorithm to its continuous counterpart in (2). Indeed, there are only two key differences: (1) we now propagate N value functions simultaneously (corresponding to N discrete modes), as opposed to just one value function. (2) We “adjust” the value function for each discrete mode to account for discrete switches (the second for-loop in the algorithm). As a result, the proposed hybrid reachability algorithm leads to a quadratic (in N) growth in the worst-case computational complexity of its continuous system counterpart.

V. CASE STUDIES

A. Running example (Dog1D):

We now apply the proposed method to compute the BRT for the running example. To implement Algorithm 1, we use a modified version of helperOC library and the level set toolbox, ToolboxLS [28], both of which are used to solve classical HJI-VI. We use a grid of 301 points over

the x dimension for each of the 3 discrete operation modes. The overall calculation takes 12.125s running on an Intel Core i5-6200U CPU @ 2.30GHz. Slices of the BRT starting in mode q_1 (the walking gait) for different time horizons are shown in Fig. 5: The intuitive solution for the optimal

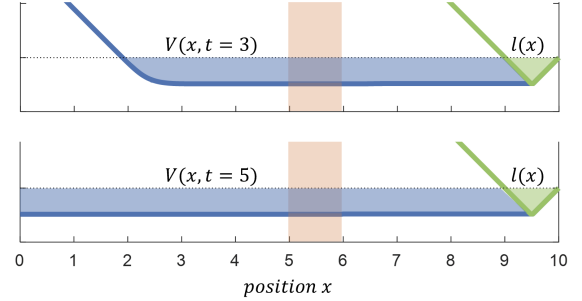


Fig. 5: Value functions for states starting in a walking gait for a 3 and 5 seconds time horizon. Area within the obstacle is shown in shaded red. Blue shade shows BRT as the subzero level of the value function. Green shade shows the target set as the subzero level of the implicit target function $l(x)$.

decision-making in this scenario is to use the walking gait everywhere except in the obstacle area. The fast walking gait allows the system to reach the target quicker, while crawling allows to expand the reachable states beyond the obstacle. The computed solution using our algorithm indeed aligns with this intuition. For example, if we consider the top value function for the 3-second time horizon in Fig. 5, we can observe that the limit of the BRT is 7m away from the target set, which coincides with the intuitive solution of walking for 1s covering 3m, then crawling under the table for 1s covering its 1m width, to finally go back to walking for 1s covering other 3m.

The bottom value function in Fig. 5 shows the BRT corresponding to a 5s time horizon. Compared to Fig. 4, where the BRT stopped growing beyond the obstacle boundary, we can see how the proposed algorithm can optimally leverage discrete transitions along with continuous control to reach the target set from a wider set of initial states.

B. Two-Aircraft Conflict Resolution:

We next consider the two-aircraft conflict resolution example presented in [26]. Here, two aircraft flying at a fixed altitude are considered. Each aircraft controls its speed; we assume that the first aircraft is controllable, while the other aircraft’s speed is uncertain (within a known interval) and hence modeled as an adversarial disturbance to ensure safety. Using relative coordinates, the continuous dynamics of the system are described by:

$$\dot{x}_r = -u + d \cos \psi_r + \omega_u y_r, \quad \dot{y}_r = d \sin \psi_r - \omega_u x_r, \quad \dot{\psi}_r = \omega_d - \omega_u,$$

where state $[x_r, y_r, \varphi_r]^T$ is the relative xy position and heading between the aircraft. u and d are the velocities of the two aircraft, and ω_u and ω_d are their turning rates.

The conflict resolution protocol consists of three different operation modes, shown in Fig. 6. The aircraft begin in mode q_1 with a straight flight ($\omega_u = \omega_d = 0$), keeping a constant relative heading. In this mode, the aircraft are on a collision course. At some time, the aircraft can begin

the collision avoidance maneuver by taking the switch σ_{12} , transitioning the system into mode q_2 and an instantaneous heading change of $\pi/2$. In mode q_2 , the aircraft undergo a circular flight path, where both aircraft use the same constant turning rate ($\omega_u = \omega_d = 1$). Once the aircraft undergo a heading change of π radians, the aircraft are forced to switch to mode q_3 , making another instantaneous $\pi/2$ turn and resuming their straight flight ($\omega_u = \omega_d = 0$). The two aircraft are now on a collision-free path. To keep track of the transition time on configuration q_2 we add an additional timer state z .

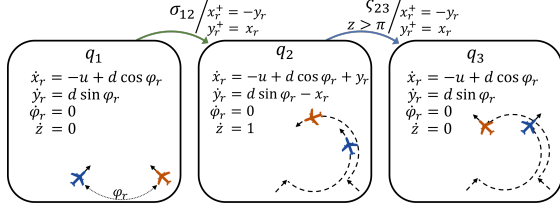


Fig. 6: Hybrid formulation for the two-aircraft conflict resolution protocol.

For this system, we are interested in finding the set of all initial states in mode q_1 from which a collision cannot be averted between the two aircraft under the above protocol, despite the best control effort. Thus, the complement of the BRT will represent the safe states for the system. For BRT calculations, we consider a circular collision target set of 5 units around the controlled aircraft. This corresponds to the two aircraft being in close proximity of each other, also referred to as “loss of separation”. We use an initial relative heading of $\varphi_r = 2\pi/3$ (shown in Fig. 6) and a time horizon of $t = 5s$. For aircraft velocities we consider $u \in [1.5, 3]$ and $d \in [2, 4]$. The calculations are carried on a $[x_r, y_r, z]$ grid of $[201, 201, 101]$ points, φ_r has null dynamics in all operation modes and is not considered in the grid.

Results for BRT starting from operation mode q_1 are shown in Fig. 7. They can be interpreted as follows: if the relative coordinates of the aircraft belong to a state outside the BRT, the collision avoidance maneuver can be initiated while ensuring a collision can always be avoided as long as the optimal discrete and continuous control is applied. The

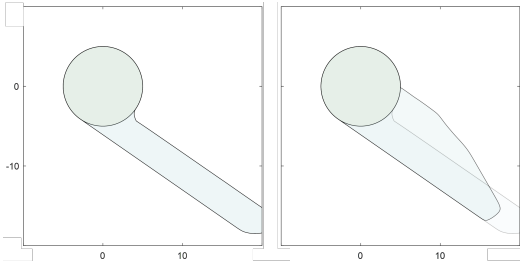


Fig. 7: Backward reachable tube for two-aircraft conflict resolution starting from mode q_1 . (Left) BRT for fixed speed of aircraft. (Right) BRT for aircraft under optimal control and disturbance.

left BRT exactly replicates the results of the case presented in [26] where both aircraft keep their speed constant at their maximum value $u = 3$ and $d = 4$, where the inside of the BRT correspond to states where the adversarial airplane can place itself behind the controlled aircraft and use its higher velocity to force a collision. However, unlike [26], we do not use any hard-coded heuristics to account for the discrete

transitions during the BRT computation. Furthermore, the right BRT considers the scenario where, in addition to the control on the transition, both aircraft control their velocities optimally to avoid/force a collision with the other aircraft. The changes in the BRT are reflected in the shaded areas, where the growth in the BRT close to the target corresponds to cases where the adversarial aircraft slows down to align itself with the controlled aircraft and then use its higher velocity to force a collision. The decrease in size near the tail corresponds to states where the blue airplane slows down to avoid a collision.

VI. HARDWARE EXPERIMENTS

We next apply our method for task-based, high-level mode planning on a real-world quadruped robot, to reach a goal position in a terrain consisting of various obstacles. The quadruped has different walking modes, such as normal walking, walking on a slope, etc., each of which is modeled as a discrete mode in the hybrid system (see Fig. 9).

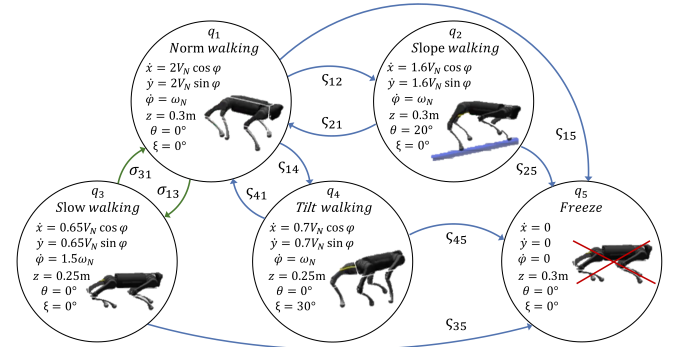


Fig. 9: Hybrid control modes for the quadruped system.

Within each discrete mode, we use simplified continuous dynamics to describe center-of-mass evolution:

$$\dot{x} = k_x V_N \sin \varphi + d_x; \quad \dot{y} = k_y V_N \cos \varphi + d_y; \quad \dot{\varphi} = k_\omega \omega_N,$$

where the state $[x, y, \varphi]^T$ represent the xy position and heading angle of the robot. $V_N = 0.25m/s$ is the fixed (normalized) linear velocity and $\omega_N \in [-0.5, 0.5]rad/s$ is the angular velocity control. k_x , k_y , and k_ω are velocity gains for different operation modes. d_x and d_y are bounded disturbances on xy velocity. Also, we use discrete state $[z, \theta, \xi]^T$ to set the body’s height, pitch, and roll angle in different operation modes for overcoming various obstacles.

Each operation mode matches a specific obstacle or terrain shown in Fig. 8(b). The quadruped begins in mode q_1 for fast walking. If the robot reaches the boundary of the slope area, the system will be forced to switch to mode q_2 with a 20° body pitch angle for slope climbing. At some time, the control may switch to mode q_3 to walk slowly with a lower body height, this allows the robot to make a narrow turn or crawl under obstacles. If the robot encounters a tilted obstacle, the system will go through a forced switch into mode q_4 to walk with a tilted body. Whenever the robot touches a ground obstacle, the system will stay in mode q_5 permanently with frozen dynamics. The quadruped needs to reason about optimally switching between these different



Fig. 8: (a) Trajectories of the quadruped safely navigating through the slope or narrow ground obstacles to reach the goal area (pink cylinder). The goal area is independent of the z position, so the robot can reach it via slope or ground route. (b) Overlaid trajectories in the real-world obstacle setup. (c, d) First-person view along the slope route (c) and the ground route (d).

walking modes in order to reach its goal area (the xy area marked as the pink cylinder in Fig. 8(a, b)) as quickly as possible without colliding with any obstacles.

BRT for this experiment is calculated on a $[x, y, \varphi]$ grid of $[40, 40, 72]$ points, over a time horizon of $t = 45s$. Having the BRT, we can acquire optimal velocity control, operation mode, and the desired discrete body states at each time. The quadruped is equipped with an Intel T265 tracking camera, allowing it to estimate its global state via visual-inertial odometry. The high-level optimal velocity control and discrete body states provided by our framework are then tracked by a low-level MPC controller that uses the centroidal dynamics of the quadruped [29].

Our experiment results are shown in Fig. 8 and can also be seen in the accompanying video. In our environment setup, the optimal (fastest) route to reach the target is via leveraging the slope on the right. The corresponding trajectory is shown in orange in Fig. 8(a) and (b). Specifically, the robot remains in the normal walking mode (blue boxes in Fig. 8(a)) and switches to the slope walking mode once near the slope (magenta boxes). When the robot approaches the end of the slope, it needs to make a tight left turn to avoid a collision with the wall ahead. Our framework is able to recognize that and makes a transition to the slow walking mode to allow for a tighter turn (green boxes). Once the turn is complete, the robot goes back in the faster walking mode. Some first-person RGB images along the robot's path are in Fig. 8(c).

In our second experiment, we put some papers on the slope, making it more slippery. This is encoded by adding a higher disturbance in the slope mode q_2 . The new BRT makes the slope path infeasible and hence the robot needs to reach the target via the (slower) ground route. The new robot trajectory is shown in light green in Fig. 8(a) and (b). Once again, apart from selecting a new safe route, the proposed framework is able to switch between different walking modes along the route to handle tight turns and slanted obstacles, as shown by the activation of the tilt walking mode (cyan boxes in Fig. 8(a)).

Finally, to test the closed-loop robustness of our method, we add human disturbance in the ground route experiment. The robot is kicked and dragged by a human during the locomotion process, as shown by red arrows in Fig. 10. Specifically, the robot was dragged to face backward, forcing

it near the tilted obstacle. However, the reachability controller is able to ensure safety by reactivating the tilt walking mode (Fig. 10(b)), demonstrating that the proposed framework is able to reason about both closed-loop continuous and discrete control inputs. Nevertheless, it should be emphasized that the presented algorithm does not solve the entirety of legged locomotion planning, but rather only provides the top level of a hierarchical planning architecture that typically include a robust footstep planner, a wholebody controller, and reliable state estimation [30]. We will further explore integrating our framework within such architectures in future.

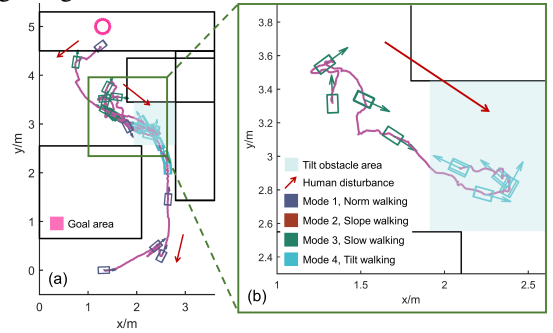


Fig. 10: (a) Robot trajectory with human disturbances. (b) Partial trajectory shows the robot autonomously switches from q_3 to q_4 after being pushed into the tilt obstacle area to ensure safety.

VII. DISCUSSION AND FUTURE WORK

We present an extension of the classical HJ reachability framework to hybrid dynamical systems with controlled and forced transitions, and state resets. Along with the BRT, the proposed framework provides optimal continuous and discrete control inputs for the hybrid system. Simulation studies and hardware experiments demonstrate the proposed method, both to reach goal areas and in maintaining safety. Our work opens up several exciting future research directions. First, we rely on grid-based numerical methods to compute the BRT, whose computational complexity scales exponentially with the number of continuous states, limiting a direct use of our framework to relatively low-dimensional systems. We will explore recent advances in learning-based methods to solve HJI-VI [31], [32] to overcome this challenge. Another interesting direction would be to extend our framework to the cases involving uncertainty in the transition surface S_i or where controlled switches have different transition surfaces. Finally, we will apply our framework on a broader range of robotics applications and systems.

REFERENCES

- [1] R. Goebel, R. G. Sanfelice, and A. R. Teel, "Hybrid dynamical systems," *IEEE control systems magazine*, vol. 29, no. 2, pp. 28–93, 2009.
- [2] A. M. Johnson, S. A. Burden, and D. E. Koditschek, "A hybrid systems model for simple manipulation and self-manipulation systems," *The International Journal of Robotics Research*, vol. 35, no. 11, pp. 1354–1392, 2016.
- [3] M. Althoff, O. Stursberg, and M. Buss, "Computing reachable sets of hybrid systems using a combination of zonotopes and polytopes," *Nonlinear Analysis: Hybrid Systems*, vol. 4, no. 2, pp. 233–249, 2010, iFAC World Congress 2008. [Online]. Available: <https://www.sciencedirect.com/science/article/pii/S1751570X09000442>
- [4] M. Althoff and B. H. Krogh, "Avoiding geometric intersection operations in reachability analysis of hybrid systems," in *Proceedings of the 15th ACM international conference on Hybrid Systems: Computation and Control*, 2012, pp. 45–54.
- [5] M. Maiga, N. Ramdani, L. Travé-Massuyès, and C. Combastel, "A comprehensive method for reachability analysis of uncertain nonlinear hybrid systems," *IEEE Transactions on Automatic Control*, vol. 61, no. 9, pp. 2341–2356, 2015.
- [6] C. Tang and M. Althoff, "Formal verification of robotic contact tasks via reachability analysis," *arXiv preprint arXiv:2307.13977*, 2023.
- [7] L. Benvenuti, D. Bresolin, A. Casagrande, P. Collins, A. Ferrari, E. Mazzi, A. Sangiovanni-Vincentelli, and T. Villa, "Reachability computation for hybrid systems with ariadne," *IFAC Proceedings Volumes*, vol. 41, no. 2, pp. 8960–8965, 2008.
- [8] P. Collins and J. Lygeros, "Computability of finite-time reachable sets for hybrid systems," in *Proceedings of the 44th IEEE Conference on Decision and Control*, 2005, pp. 4688–4693.
- [9] X. Chen, E. Ábrahám, and S. Sankaranarayanan, "Flow*: An analyzer for non-linear hybrid systems," in *Computer Aided Verification: 25th International Conference, CAV 2013, Saint Petersburg, Russia, July 13-19, 2013. Proceedings 25*. Springer, 2013, pp. 258–263.
- [10] X. Chen, E. Abraham, and S. Sankaranarayanan, "Taylor model flowpipe construction for non-linear hybrid systems," in *2012 IEEE 33rd Real-Time Systems Symposium*. IEEE, 2012, pp. 183–192.
- [11] N. Kochdumper and M. Althoff, "Reachability analysis for hybrid systems with nonlinear guard sets," ser. HSCC '20. Association for Computing Machinery, 2020.
- [12] S. Kong, S. Gao, W. Chen, and E. Clarke, "dreach: δ -reachability analysis for hybrid systems," in *Tools and Algorithms for the Construction and Analysis of Systems: 21st International Conference, TACAS 2015, Held as Part of the European Joint Conferences on Theory and Practice of Software, ETAPS 2015, London, UK, April 11-18, 2015, Proceedings 21*. Springer, 2015, pp. 200–205.
- [13] W. Damm, S. Disch, H. Hungar, S. Jacobs, J. Pang, F. Pigorsch, C. Scholl, U. Waldmann, and B. Wirtz, "Exact state set representations in the verification of linear hybrid systems with large discrete state space," in *International Symposium on Automated Technology for Verification and Analysis*. Springer, 2007, pp. 425–440.
- [14] G. Frehse, C. Le Guernic, A. Donzé, S. Cotton, R. Ray, O. Lebeltel, R. Ripado, A. Girard, T. Dang, and O. Maler, "Spaceex: Scalable verification of hybrid systems," in *Proc. 23rd International Conference on Computer Aided Verification (CAV)*, ser. LNCS, S. Q. Ganesh Gopalakrishnan, Ed. Springer, 2011.
- [15] C. Le Guernic and A. Girard, "Reachability analysis of linear systems using support functions," *Nonlinear Analysis: Hybrid Systems*, vol. 4, no. 2, pp. 250–262, 2010.
- [16] G. Frehse and R. Ray, "Flowpipe-guard intersection for reachability computations with support functions," *IFAC Proceedings Volumes*, vol. 45, no. 9, pp. 94–101, 2012.
- [17] R. Alur, C. Courcoubetis, T. A. Henzinger, and P.-H. Ho, "Hybrid automata: An algorithmic approach to the specification and verification of hybrid systems," in *International Hybrid Systems Workshop*. Springer, 1991, pp. 209–229.
- [18] T. A. Henzinger, P.-H. Ho, and H. Wong-Toi, "A user guide to hytech," in *International Workshop on Tools and Algorithms for the Construction and Analysis of Systems*. Springer, 1995, pp. 41–71.
- [19] S. Yovine, "Kronos: A verification tool for real-time systems," *Int. J. Softw. Tools Technol. Transf.*, vol. 1, no. 1-2, pp. 123–133, 1997.
- [20] O. Maler, A. Pnueli, and J. Sifakis, "On the synthesis of discrete controllers for timed systems," in *STACS 95: 12th Annual Symposium on Theoretical Aspects of Computer Science Munich, Germany, March 2-4, 1995 Proceedings 12*. Springer, 1995, pp. 229–242.
- [21] S. Bansal, M. Chen, S. Herbert, and C. J. Tomlin, "Hamilton-Jacobi Reachability: A brief overview and recent advances," in *IEEE Conference on Decision and Control (CDC)*, 2017.
- [22] A. Dhinakaran, M. Chen, G. Chou, J. C. Shih, and C. J. Tomlin, "A hybrid framework for multi-vehicle collision avoidance," in *Conference on Decision and Control*, 2017, pp. 2979–2984.
- [23] J. H. Gillula, G. M. Hoffmann, H. Huang, M. P. Vitus, and C. J. Tomlin, "Applications of hybrid reachability analysis to robotic aerial vehicles," *The International Journal of Robotics Research*, vol. 30, no. 3, pp. 335–354, 2011.
- [24] C. Tomlin, J. Lygeros, and S. Sastry, "Computing controllers for nonlinear hybrid systems," in *Hybrid Systems: Computation and Control: Second International Workshop, HSCC'99 Berg en Dal, The Netherlands, March 29-31, 1999 Proceedings 2*. Springer, 1999, pp. 238–255.
- [25] I. Mitchell and C. J. Tomlin, "Level set methods for computation in hybrid systems," in *International workshop on hybrid systems: Computation and control*. Springer, 2000, pp. 310–323.
- [26] —, "Level set methods for computation in hybrid systems," in *International workshop on hybrid systems: Computation and control*. Springer, 2000, pp. 310–323.
- [27] J. J. Choi, A. Agrawal, K. Sreenath, C. J. Tomlin, and S. Bansal, "Computation of regions of attraction for hybrid limit cycles using reachability: An application to walking robots," *IEEE Robotics and Automation Letters*, vol. 7, no. 2, pp. 4504–4511, 2022.
- [28] I. Mitchell, "A toolbox of level set methods," <http://www.cs.ubc.ca/mitchell/ToolboxLS/toolboxLS.pdf>, Tech. Rep. TR-2004-09, 2004.
- [29] D. Kim, J. D. Carlo, B. Katz, G. Bledt, and S. Kim, "Highly dynamic quadruped locomotion via whole-body impulse control and model predictive control," 2019.
- [30] J. Norby and A. M. Johnson, "Fast global motion planning for dynamic legged robots," in *2020 IEEE/RSJ International Conference on Intelligent Robots and Systems (IROS)*. IEEE, 2020, pp. 3829–3836.
- [31] S. Bansal and C. J. Tomlin, "DeepReach: A deep learning approach to high-dimensional reachability," in *IEEE International Conference on Robotics and Automation (ICRA)*, 2021.
- [32] A. Lin and S. Bansal, "Generating formal safety assurances for high-dimensional reachability," 2022. [Online]. Available: <https://arxiv.org/abs/2209.12336>
- [33] J. Lygeros, "On reachability and minimum cost optimal control," *Automatica*, vol. 40, no. 6, pp. 917–927, 2004.

VIII. APPENDIX

A. Proof of Theorem 1

We start with an analogous formulation to HJ reachability with a target function $l(x)$ such that the target set is defined as its sub-zero level set, $\mathcal{L} = \{(x) : l(x) \leq 0\}$. The BRT seeks to find all states that could enter \mathcal{L} at any point within the time horizon. This is computed by finding the minimum distance to \mathcal{L} over time.

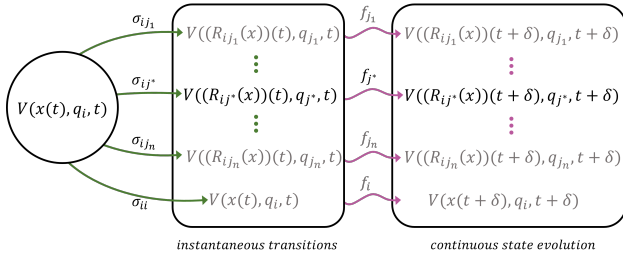
The value function is defined as the cost incurred under optimal discrete and continuous controls that minimizes distance to the target and optimal disturbances that maximizes it. We first consider the case when the state belongs to the interior of the domain S_i . The value function is given as:

$$V(x, q_i, t) = \max_{d \in D} \min_{u \in U} \min_{\sigma_{ij}} \min_{s \in [t, T]} l(x(s)) \quad (10)$$

With terminal time condition given by:

$$V(x, q_i, T) = l(x) \quad (11)$$

The optimal decision making for discrete transitions is pictorially shown in the figure below. The discrete transitions



are shown in green arrows and continuous control flow are indicated by purple trajectories. We also add a “dummy” discrete transition, σ_{ii} , that keeps the system in the current discrete mode. As per (10), the overall value function is given by the minimum cost across all these possible trajectories of the system. From here, we consider two different cases:

Case 1: If the system switches to a new discrete mode j^* , the continuous state immediately transitions to R_{ij^*} . In this case, the optimal cost incurred by the system from the new state $(R_{ij^*}(x), q_{j^*})$ is, by definition, given as $V(R_{ij^*}(x), q_{j^*}, t)$. Thus, the optimal cost across all possible discrete transitions is given as:

$$V(x, q_i, t) = \min_{\sigma_{ij}} V(R_{ij}(x), q_j, t) \quad (12)$$

Case 2: The system evolves in the same mode q_i , i.e., it takes the dummy switch σ_{ii} . In this case, for a small time step δ and using the dynamic programming principle for the cost function in (10), we have:

$$\begin{aligned} V(x, q_i, t) &= \max_{d \in D} \min_{u \in U} \min \left\{ \min_{s \in [t, t+\delta]} l(x(s)), \right. \\ &\quad \left. V(x(t+\delta), q_i, t+\delta) \right\} \\ &\approx \max_{d \in D} \min_{u \in U} \min \{ l(x(t)), V(x(t+\delta), q_i, t+\delta) \} \end{aligned} \quad (13)$$

Approximating the value function at the next time step with a first order Taylor expansion:

$$\begin{aligned} V(x(t+\delta), q_i, t+\delta) &\approx V(x, q_i, t) + \\ &\quad D_t V(x, q_i, t) \delta + \nabla V(x, q_i, t) \cdot \delta x, \end{aligned} \quad (14)$$

where the change in the state δx can be approximated as $f_i(x, u, d)\delta$. Ignoring the higher order terms and plugging the Taylor expansion in (13):

$$\begin{aligned} V(x, q_i, t) &= \min \{ l(x(t)), \\ &\quad V(x, q_i, t) + D_t V(x, q_i, t) \delta + \max_{d \in D} \min_{u \in U} \nabla V(x, q_i, t) \cdot f_i(x, u, d) \delta \} \end{aligned} \quad (15)$$

The optimal value function is given by the minimum across the two cases:

$$\begin{aligned} V(x, q_i, t) &= \min \{ l(x), \\ &\quad V(x, q_i, t) + D_t V(x, q_i, t) \delta + \max_{d \in D} \min_{u \in U} \nabla V(x, q_i, t) \cdot f_i(x, u, d) \delta, \\ &\quad \min_{\sigma_{ij}} V(R_{ij}(x), q_{ij}, t) \} \end{aligned} \quad (16)$$

Subtracting the value function $V(x, q_i, t)$ from both sides:

$$\begin{aligned} 0 &= \min \{ l(x(t)) - V(x, q_i, t), \\ &\quad \delta (D_t V(x, q_i, t) + \max_{d \in D} \min_{u \in U} \nabla V(x, q_i, t) \cdot f_i(x, u, d)), \\ &\quad \min_{\sigma_{ij}} V(R_{ij}(x), q_{ij}, t) - V(x, q_i, t) \} \end{aligned} \quad (17)$$

Since the above hold for all $\delta > 0$ we must have:

$$\begin{aligned} 0 &= \min \{ l(x(t)) - V(x, q_i, t), \\ &\quad D_t V(x, q_i, t) + \max_{d \in D} \min_{u \in U} \nabla V(x, q_i, t) \cdot f_i(x, u, d), \\ &\quad \min_{\sigma_{ij}} V(R_{ij}(x), q_j, t) - V(x, q_i, t) \} \end{aligned} \quad (18)$$

Note that here we have presented an informal proof based on the Taylor series expansion of the value function; a more rigorous proof of HJI-VI for continuous evolution can be found in [33].

For states outside the domain of the discrete mode q_i (i.e., $x \in S_i^C$), our discrete decision is over the set of available forced switches ς_{ik} . For this case the proof is analogous to the Case 1 previously considered, but without the option to stay in q_i . The value function is then given by:

$$V(x, q_i, t) = \min_{\varsigma_{ik}} V(R_{ik}(x), q_k, t) \quad (19)$$